Inorganic Chemistry

Article

pubs.acs.org/IC

In Situ Study of the Solid-State Formation of $U_{1-x}Am_xO_{2\pm\delta}$ Solid Solution

Florent Lebreton,[†,§] Renaud C. Belin,[‡] Damien Prieur,[†] Thibaud Delahaye,*[,†] and Philippe Blanchart[§]

[†]CEA, DEN, DTEC/SDTC/LEMA, F-30207 Bagnols-sur-Cèze Cedex, France

[‡]CEA, DEN, DEC/SPUA/LMPC, F-13108 Saint-Paul-Lez-Durance, France

[§]GEMH, ENSCI, 87065 Limoges, France

ABSTRACT: In order to reduce the nuclear waste inventory and radiotoxicity, $U_{1-x}Am_xO_{2\pm\delta}$ materials are promising fuels for heterogeneous transmutation. In this context, they are generally fabricated from $UO_{2+\delta}$ and $AmO_{2-\delta}$ dioxide powders. In the subsequent solid solution, americium is assumed to be trivalent whereas uranium exhibits a mixed-valence (+IV/+V) state. However, no formation mechanisms were ever evidenced and, more particularly, it was not possible to know whether the reduction of Am(IV) to Am(III) occurs before the solid-solution formation, or only once it is established. In this study, we used high-temperature X-ray diffraction on a $UO_{2\pm\delta}/AmO_{2-\delta}$ (15 mol %) mixture to observe in situ the formation of the $U_{1-x}Am_xO_{2\pm\delta}$ solid solution. We show that $UO_{2+\delta}$ is, at relatively low temperature (<700 K), oxidized to $U_4O_{9-\delta}$, which is likely to be caused by oxygen release from the simultaneous $AmO_{2-\delta}$ reduction to cubic $Am_2O_{3\pm\delta}$. Cubic $Am_2O_{3+\delta}$ then transforms to hexagonal Am_2O_3 at 1300 K. Thus, the initial Am(IV) is fully reduced to Am(III) before the solid solution starts forming at 1740 K. The UO_2 fluorite phase vanishes after 4 h at 1970 K, indicating that the formation of the solid solution is completed, which proves that this solid solution is formed after the complete reduction of Am(IV) to Am(III).

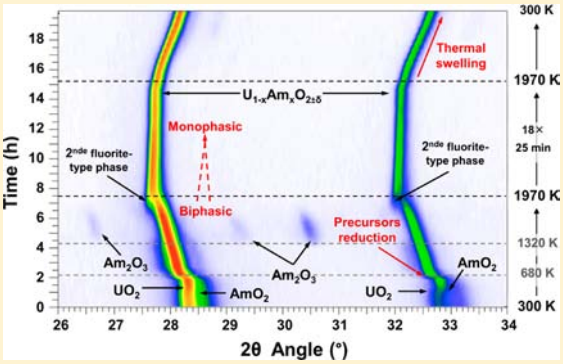

I. INTRODUCTION

Np, Am, and Cm, which are minor actinides (MA), are generated in small quantities (<1 wt % of the fuel) in nuclear fuels during irradiation in reactors. Because of their high activity and long life, they represent the majority of the radiotoxicity and heat generation of nuclear waste after 100 years, when plutonium is reprocessed through mixed oxide (MOX) fuels. To recycle them, transmutation into short-lived or stable elements in a fast neutron reactor is considered.[1] Two ways are commonly investigated. For homogeneous recycling, up to 5 wt % of MA are added to MOX fuels introduced into the core.[2,3] In the case of heterogeneous transmutation, which is currently the main focus of research, a greater amount of MA is added to depleted UOX fuels and placed in specific assemblies in the periphery of the core.[4] These materials are known as MABB (MA-bearing blanket) fuels. Among the MA, the high radiotoxicity and relative abundance of ^{241}Am have prompted research on the fabrication of Am-bearing uranium fuels (described as $U_{1-x}Am_xO_{2\pm\delta}$).[5] In that context, various manufacturing processes are being developed in our research facility (i.e., powder metallurgy involving reactive[4,6,7] or conventional sintering[8]).

At an industrial scale, uranium is used as a fuel for nuclear reactors, notably in the form of UO_2 ceramic pellets. These fuels are generally prepared by sintering in a reducing atmosphere (H_2) for 4 h at 1973 K, which allows dense and almost-stoichiometric pellets to be obtained. But compared to uranium oxides, americium oxides have drastically different thermodynamic properties, such as much higher oxygen potentials. Consequently, americium and uranium oxides exhibit different oxidation/reduction behaviors. In contrast, both dioxides crystallize in the same fluorite-type structure with a room-temperature (RT) lattice parameter of 5.4705 Å for UO_2[9,10] and ranging from 5.372 Å to 5.377 Å, depending on powder purity or stoichiometry for AmO_2.[11,12]

On the one hand, uranium is more stable in the U(IV) state, as well as in higher oxidation states (such as +V or +VI),[13] implying that UO_2 is easily oxidized to hyperstoichiometric $UO_{2+\delta}$, or even U_4O_9 or U_3O_8. In the case of $UO_{2+\delta}$, a mixed valence (+IV/+V) of uranium compensates for oxygen hyperstoichiometry. Until δ = 0.01, O atoms are introduced in ($^1/_2$ $^1/_2$ $^1/_2$) or ($^1/_2$ 0 0) cubic-coordinated interstitial sites. For higher δ values, defect clusters are formed, associating oxygen vacancies in ($^1/_4$ $^1/_4$ $^1/_4$) sites with oxygen in interstitial sites shifted toward the ⟨111⟩ and ⟨110⟩ directions.[14−16] However, the uranium sublattice remains unchanged, whatever the oxygen-to-metal (O/M) ratio. On the other hand, americium is stabilized in lower valence states than +IV,[13] favoring the reduction of AmO_2 to hypostoichiometric $AmO_{2-\delta}$, or more-reduced phases. Thus, americium sesquioxide is the stable form under ambient conditions, with structures

Received: May 29, 2012
Published: August 21, 2012

   dx.doi.org/10.1021/ic301124d | *Inorg. Chem.* 2012, 51, 9369−9375

corresponding to those known as A-, B-, and C-type lanthanide sesquioxides. The stable structures of americium sesquioxide are C-type $Am_2O_{3+\delta}$ (cubic), in which americium has a mixed valence (+III/+IV) to accommodate for the O/M ratio, or A-type Am_2O_3 (hexagonal)[12,17,18] with only Am(III). B-type $Am_2O_{3+\delta}$ (monoclinic) may also exist, but its occurrence is still debated as it was only observed as a secondary phase.[11,12,19]

Considering properties of $UO_{2+\delta}$ and $AmO_{2-\delta}$, a $U_{1-x}Am_xO_{2\pm\delta}$ solid solution cannot be described as a UO_2 phase in which Am(IV) partially substitutes for U(IV). Moreover, this solid solution is supposed to exist in both hypostoichiometric and hyperstoichiometric states and, under conditions such as those frequently used to sinter UO_2 fuels, i.e., 4 h at ~2000 K under Ar/H_2 (5%), americium oxide can undergo reduction to Am metal, eventually leading to partial sublimation.[18] Thus, a $U_{1-x}Am_xO_{2\pm\delta}$ solid solution should not be synthesized by a solid-state route using the typical UO_2 sintering conditions. Numerous studies published on this subject[4,20,21] showed that dense and homogeneous samples can be obtained using a heat treatment composed of slow heating and cooling rates (3 K min^{-1}) and a 4-h sintering plateau at 2023 K in a reducing atmosphere controlled by a mixture of Ar/H_2 (4%) and Ar/O_2 (10 to 190 ppm). More specifically, the influence of oxygen potential on both density and macroscopic deformation of $U_{1-x}Am_xO_{2\pm\delta}$ pellets fabricated by reactive sintering was described.[20]

Recently, several X-ray absorption spectroscopy (XAS) studies were reported on $U_{1-x}Am_xO_{2\pm\delta}$.[6,22,23] Prieur et al. and Nishi et al. notably evidenced the presence of only Am(III) and mixed U(IV/V) in the final $U_{1-x}Am_xO_{2\pm\delta}$ solid solution sintered under a reducing atmosphere. Regardless of the Am/(U + Am) ratio, the U(IV/V) mixed valence ensures structure electroneutrality, as similar U(V) and Am(III) amounts are obtained, leading to a $U(+IV)_{(1-x-x')}U^{+V}_{x'}Am^{+III}_xO_{2+(x'-x)/2}$ solid solution with close x and x'. These molar fractions are not strictly identical and dependent on the sintering atmosphere. The study of $U_{1-x}Am_xO_{2\pm\delta}$ reactive sintering in an argon atmosphere yielded similar results, even if neither the formation of solid solution nor the sintering were complete.[7] Two phenomena can explain such a charge distribution:

- On the one hand, during the UO_2/AmO_2 solid-state reaction, the cationic interdiffusion of U(IV) and Am(IV) could take place in eight-coordination, leading to a fluorite solid solution. Full reduction of Am(IV) to Am(III) may be explained by a charge transfer between Am(IV) and U(IV) via an electron transfer from uranium to americium. Such a mechanism has notably been established for a $U_{1-x}Pu_xO_{2\pm\delta}$ solid solution.[24] In complement, relativistic calculations show that the Fermi level of AmO_2 is lower than that of UO_2, which is in agreement with a charge transfer from UO_2 to AmO_2.[25]
- On the other hand, the total reduction of Am(+IV) to Am(+III) may occur before solid-solution formation, because of the high americium oxygen potential Å, leading to a phase transformation from $AmO_{2-\delta}$ to Am_2O_3. In that case, Am(III) and U(IV) interdiffuse, while the partial oxidation of U(IV) to U(V) maintains the electroneutrality of the structure, as well as an O/M ratio close to 2. By analogy with U−Ln−O systems,[26−28] U(IV) cation substitution by Am(III) could induce the partial oxidation of U(IV) in U(V) to ensure structure electroneutrality. Studies on $U_{1-x}Ln_xO_2$, with a trivalent lanthanide show the partial oxidation of the U(IV) to U(V) or U(VI) via charge compensation to ensure the electroneutrality of the structure.[26,29,30] This process supposes the absence of oxygen vacancies during the solid-state reaction, as was previously demonstrated.[6]

Recently, an in situ high-temperature X-ray diffraction (HT-XRD) study of AmO_2 under reducing atmosphere was conducted up to 1840 K.[19] During thermal treatment, several phase transformations occurring while fluorite-type AmO_2 is reduced to hexagonal A-type Am_2O_3 were evidenced as a function of temperature. This method proved to be very convenient to study phase transformation phenomena in situ. Here, we followed the same procedure on a mixture of UO_2 and AmO_2 powders in order to investigate the formation of the $U_{1-x}Am_xO_{2\pm\delta}$ solid solution during solid-state synthesis, i.e., during reactive sintering. The results are presented and discussed hereafter. Since $U_{0.85}Am_{0.15}O_{2\pm\delta}$ is the current reference MABB fuel for heterogeneous transmutation,[4,7] this composition was chosen in the present work.

II. EXPERIMENTAL SECTION

II.1. Sample. $UO_{2+\delta}$ powder was supplied by SICN Veurey-Voroize and is composed of natural uranium, with thorium as the only impurity (see Table 1). The scanning electron microscopy (SEM) micrographs in Figure 1 show that it is composed of spherical agglomerates of submicronic particles, which is a typical morphology obtained with the wet synthesis route used to produce this powder. Laser granulometry (Figure 2) shows that it is mostly composed of small particles, with the d_{50} and d_{90} relative granulometric factors being, respectively, 0.70(1) and 6.9(1) μm. This statement, as well as a specific area value of 5.6(1) m^2 g^{-1} (measured by the BET method), imply a relatively high reactivity. Thus, this is a suitable powder for the formation of a solid solution via a solid-state reaction.

Table 1. $UO_{2+\delta}$ and $AmO_{2-\delta}$ Precursor Powder Characteristics Obtained by Thermo-ionized Mass Spectrometry (TIMS), Inductively Coupled Plasma−Quadripole Mass Spectrometry (ICP-QMS), and Inductively Coupled Plasma−Atomic Emission Spectrometry (ICP-AES)

			method
	UO_2 Powder		
isotopic composition (at%)	^{234}U	0.006(1)	TIMS
	^{235}U	0.72(1)	TIMS
	^{238}U	99.27(3)	TIMS
impurities (wt%)	Th	0.11(1)	ICP-QMS
date		04/2003	
	AmO_2 Powder		
isotopic composition (at %)	^{241}Am	98.84 (1)	TIMS
	^{242}Am	<0.02	TIMS
	^{243}Am	1.25 (1)	TIMS
impurities (wt %)	Ce	1.7 (5)	ICP-AES
	Na	0.57 (17)	ICP-AES
	Nd	0.49 (14)	ICP-AES
	Fe	0.38 (11)	ICP-AES
	Np	0.2	calculated
date	04/2010		

The AmO_2 powder was obtained by an oxalate precipitation in the ATALANTE facility and contains, as seen in Table 1, a larger amount of impurities (>3 wt %). These impurities might be detrimental to reactive sintering. Indeed, it may affect the densification process or the solid-solution formation by creating additional porosity. Isotopic

dx.doi.org/10.1021/ic301124d | Inorg. Chem. 2012, 51, 9369−9375

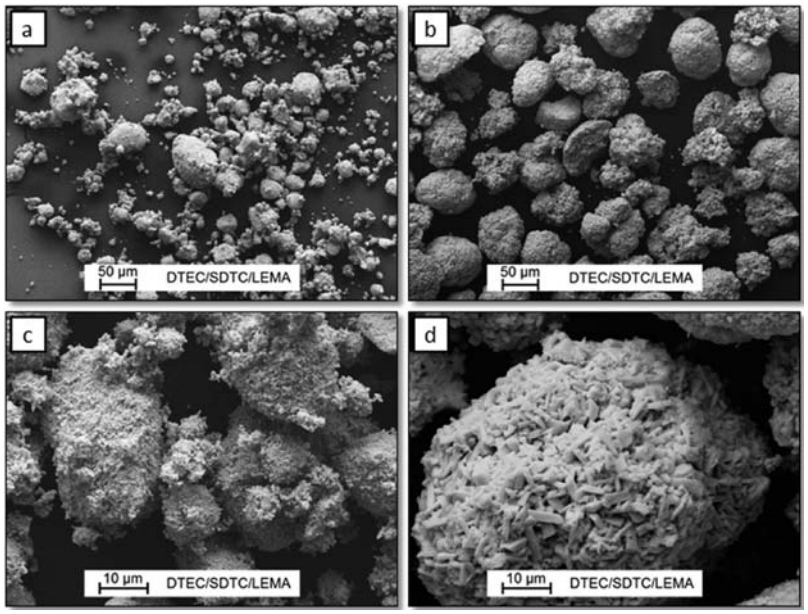

Figure 1. Scanning electron microscope (SEM) micrographs in secondary electron mode of (a and c) $UO_{2+\delta}$ and (b and d) $AmO_{2-\delta}$ precursor powders.

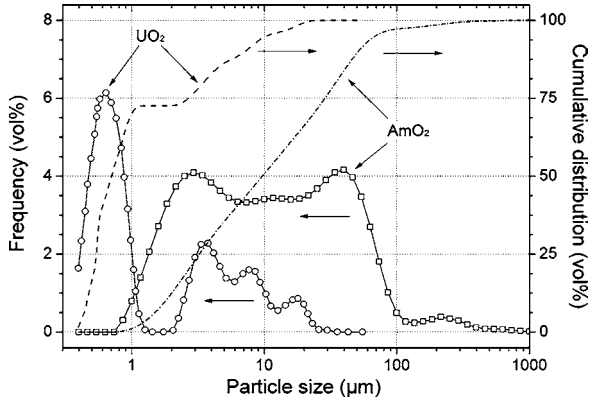

Figure 2. Particle size frequency and cumulative distributions obtained by laser granulometry (Fraunhofer model).

composition of AmO_2 powder mostly includes the ^{241}Am isotope, which has high α and γ activities (1.3×10^{11} Bq g^{-1}, compared to the 2.5×10^4 Bq g^{-1} activity of ^{Nat}U). This isotope, via self-irradiation effects, induces macroscopic swelling and lattice parameter expansion.[11] SEM micrographs (Figure 1) show powder morphology similar to that of UO_2, composed of spherical agglomerates of submicronic particles. Agglomerates observed here are however larger, which is confirmed by laser granulometry measurements presented in Figure 2. Relative granulometric factors are ~10 times higher, with d_{50} and d_{90} being, respectively, 8.6(1) and 46.4(5) μm. This powder needs at least one milling step before use as a solid-state route precursor in order to allow homogenization of the americium distribution in the powder mixture.

The $UO_{2+\delta}/AmO_{2-\delta}$ samples were prepared in hot cells at the CEA Marcoule ATALANTE facility. First, a powder mixture was prepared by a two-step ball-milling using a Retsch ball miller. This process ensures a homogeneous distribution of $AmO_{2-\delta}$ in the powder and a defined Am/(U + Am) ratio of 0.15. As-prepared powder was pelletized into disks (1.5 mm height for a diameter of 5.2 mm), ground to powder just before measurements. This pelletizing creates intimate contact between precursors and increases the number of interdiffusion sites and thus the reaction surface, even in the final powdered sample. Since the heating strip used for XRD measurements is efficient only over a local range, if disks were used as HT-XRD samples, they would have experienced a temperature gradient, leading to high measurement uncertainties.

II.2. Equipment and Method. Measurements were carried out in the LEFCA facility (CEA Cadarache) using a fully nuclearized HT-XRD setup described previously.[19] XRD diagram acquisitions were made during 25-min isothermal plateaus from 25° 2θ to 125° 2θ (Cu anticathode: Kα_1: λ = 1.5406 Å + Kα_2: λ = 1.5444 Å), using a counting time of 0.3 s and 0.02° steps. To easily compare both studies, these conditions are identical to those used for the AmO_2 study.[19] Data refinement and lattice parameter calculation were performed using the Pawley method, based on a fundamental parameter approach, on the DIFFRACplus TOPAS V4 software[31] (further details on the method were previously given[19]). The thermal cycle used is composed of three stages: heating, plateau, and cooling. During heating, measurements were taken from 600 K to 1940 K, with steps of 100 K. At this temperature, 18 successive 25-min plateaus were performed, for a total duration of 8 h. As this study focuses on solid solution formation, the cooling period will not be described here. A reducing atmosphere was maintained during measurements by the use of flowing He/H_2 (5%). Therefore, the complete thermal cycle used for the experiment is similar to that commonly used to sinter $U_{1-x}Am_xO_{2\pm\delta}$ fuels.[4] Oxygen potential was also calculated using the Wheeler and Jones formula[32] considering an amount of residual H_2O close to 5 ppm, and is comprised between −510 and −630 kJ mol^{-1}, respectively at RT and 1970 K.

III. RESULTS

Figure 3 gives isodensity mapping of XRD patterns recorded during the entire experiment between 26° 2θ and 34° 2θ. This 2θ range allows the main peaks of all phases considered in the study to be distinguished: fluorite-type UO_2 and AmO_2, as well as A-, B-, or C-type Am_2O_3. Based on this mapping, it is clear that at least one cubic structure is maintained during the entire measurement. The entire cycle is divided here into five domains (from I to V).

At RT, the most intense contribution is obviously attributed to $UO_{2+\delta}$, with a high-angle shoulder due to $AmO_{2-\delta}$ and corresponding to an expected lower lattice parameter. In Domain I (i.e., for temperature up to 680 K), no deviation of $UO_{2+\delta}$ peaks is noted, after which a large deviation occurs. In Domains II and III, from 780 K to 1970 K, the UO_2 lattice

dx.doi.org/10.1021/ic301124d | Inorg. Chem. 2012, 51, 9369−9375

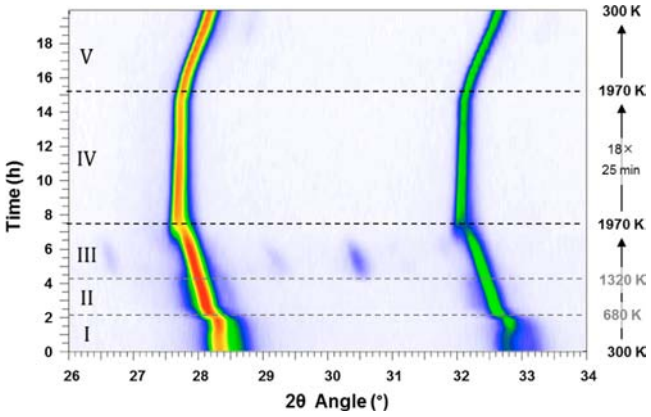

Figure 3. Complete isodensity map of XRD peak intensity of the UO_2/AmO_2 (15%) sample between 26° 2θ and 34° 2θ, as a function of time.

parameter expands with temperature, as well as does, up to 1210 K, that of AmO_2, whose lattice parameter expansion is larger than that of UO_2. Thus, the AmO_2 lattice parameter overwhelms that of UO_2 at 890 K and is then visible as a low-angle shoulder on $UO_{2+\delta}$ peaks. Between 680 and 1320 K, a large expansion is observed, which can be associated with the phase transformation of $Fm\bar{3}m$ AmO_2 to $Ia\bar{3}$ C′-type Am_2O_3, XRD patterns of these two structures being only distinguished via $Ia\bar{3}$ superlattice reflections.[12,19] Since the initial mixture contained only 15% of $AmO_{2-\delta}$, $Ia\bar{3}$ superlattice reflections might be too faint to be observed here. Consequently, the large and sudden lattice parameter expansion is the only clue permitting a strict distinction between $Fm\bar{3}m$ and $Ia\bar{3}$ structures. In Domain III, hexagonal A-type Am_2O_3 peaks are visible between 1320 K and 1840 K (see Figure 4), with an

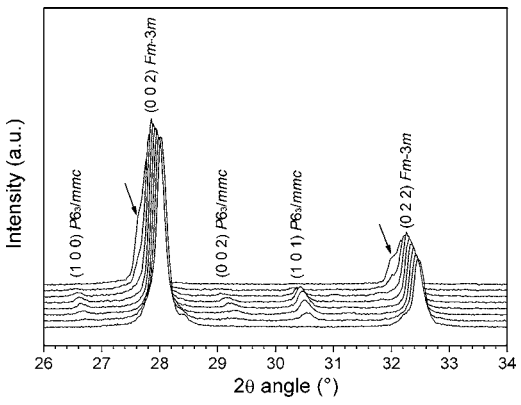

Figure 4. Excerpt of XRD patterns between 26° 2θ and 34° 2θ with increasing temperature (from bottom to top: 1210, 1320, 1420, 1530, 1630, 1740, 1840, and 1940 K) showing the hexagonal A-type Am_2O_3 phase ($P6_3/mmc$) emergence and disappearance and $U_{1-x}Am_xO_{2\pm\delta}$ solid-solution formation ($Fm\bar{3}m$) as a shoulder at low angles (indicated with arrows) of isostructural UO_2 peaks.

intensity maximum at 1530 K. Simultaneously with the emergence of the A-type Am_2O_3 peak, the AmO_2 lattice parameter decreases and is found to be close to that of UO_2. This phase remains present up to 1630 K, whereas hexagonal A-type Am_2O_3 peaks are no longer visible at 1940 K.

At 1740 K, peaks are observed at lower angles than those of UO_2 (Figure 4). At 1840 K, these peaks are more precisely defined and can clearly be associated with a new fluorite-type phase. Peak intensities of this new phase progressively increase in Domain IV, corresponding to the 1970 K-plateau, while their full width at half-maximum (fwhm) decreases, which leads to the emergence of better-defined peaks (see Figure 5).

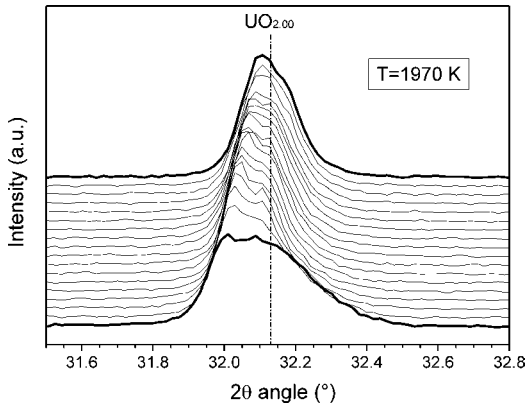

Figure 5. Excerpt of XRD patterns during plateau at 1973 K (bottom: beginning of plateau, top: after 7 h of plateau).

Meanwhile, initial peaks corresponding to the UO_2 phase drop off, and this phase vanishes after 4 h at 1973 K. Only the second fluorite phase remains visible until cooling to RT (Domain V), with a lattice parameter equal to 5.480(1) Å.

IV. DISCUSSION

IV.1. Precursors. *IV.1.1. Initial $UO_{2+\delta}$ and $AmO_{2-\delta}$ precursors.* The lattice parameter at RT is equal to 5.463(1) Å for $UO_{2+\delta}$. The comparison with the admitted value for stoichiometric UO_2, 5.4705 Å, suggests an oxygen hyper-stoichiometry, which is known to induce lattice parameter decrease.[9] This result is not surprising for uranium oxide, which is not supposed to be stable in hypostoichiometric state at RT. Based on the relationship between lattice parameter and oxygen stoichiometry in $UO_{2+\delta}$ at RT given by Teske et al.,[9] the O/M ratio is estimated at 2.06(1).

Concerning $AmO_{2-\delta}$, its lattice parameter is 5.409(1) Å. The influence of self-irradiation effects has to be taken into account, in addition to those of impurities and the O/M ratio. Self-irradiation is known to cause an increase of 0.27(4)% after more than 3 months of storage.[11,12,19,20] This sample was stored for 2 years, which allows a theoretical "undamaged" lattice parameter of 5.394(3) Å to be calculated. The resulting large discrepancy with the given value for stoichiometric AmO_2 of 5.373 Å,[11,12] i.e., 0.2 Å, corresponding to 3.3%, is easily attributable to the effects of impurities and of oxygen hypostoichiometry. Nevertheless, this remains a qualitative statement, because it is impossible to decouple these effects.

IV.1.2. $UO_{2+\delta}$ and $AmO_{2-\delta}$ Behavior in Domain I (T < 680 K). $UO_{2+\delta}$ and $AmO_{2-\delta}$ lattice parameters are given in Figure 6, as a function of temperature for Domains I−III.

Concerning americium oxide, its behavior during heating is compared to that observed for pure $AmO_{2-\delta}$ under identical conditions.[19] First, a large lattice parameter increase is expected at 680 K, corresponding to the reduction to C′-type $Am_2O_{3+\delta}$ ($Ia\bar{3}$). $Ia\bar{3}$ superlattice peaks are not visible due to the low amount of americium oxide in the sample, thus the transformation from $Fm\bar{3}m$ $AmO_{2-\delta}$ to $Ia\bar{3}$ $Am_2O_{3+\delta}$ structure cannot be precisely identified. In the present work, this phenomenon starts at the same temperature, but proceeds at a

dx.doi.org/10.1021/ic301124d | Inorg. Chem. 2012, 51, 9369−9375

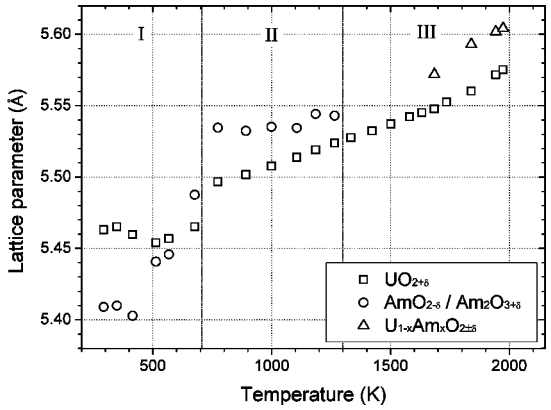

Figure 6. Variation of lattice parameters with temperature: (□) $UO_{2+\delta}$, (○) $AmO_{2-\delta}$ then C-type $Am_2O_{3+\delta}$, and (△) $U_{1-x}Am_xO_{2\pm\delta}$.

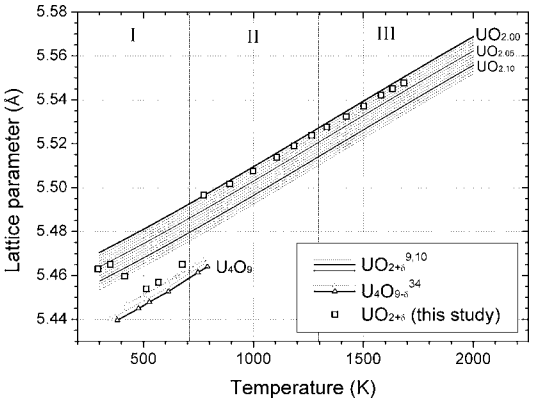

Figure 7. Comparison between (□) $UO_{2+\delta}$ lattice parameter obtained by HT-XRD pattern refinement and lattice parameter thermal expansion of several $UO_{2+\delta}$ phases (data extrapolated from measurements as a function of O/M ratio by Teske et al.[9] and the thermal expansion coefficient (TEC) calculated by Yamashita et al.[10] admitting that $UO_{2+\delta}$ TEC remains constant with O/M ratios over the considered stoichiometry/temperature range) and of $U_4O_{9-\delta}$, data taken from Naito[34] for O/M ratios equal to 2.23, 2.24, and 2.25.

slower rate. It can only be considered complete at 770 K. Considering that both the initial AmO_2 powder and the experimental conditions (data acquisition time, temperature, and atmosphere) are identical to those used for the AmO_2 study, this slower rate is likely to result from the presence of $UO_{2+\delta}$. Americium oxide particles are here diluted in a $UO_{2+\delta}$ matrix, decreasing direct contact with the atmosphere. Considering the initial low amount of oxygen in the atmosphere, it may significantly change the oxygen potential, especially when considering the local environment of oxide particles. This could explain why $AmO_{2-\delta}$ reduction to $Am_2O_{3+\delta}$ still begins at the same temperature, but occurs at a slower rate than that of pure americium oxide.

In Domain I, the uranium phase exhibits a peculiar behavior. In this temperature range, two phenomena are expected: thermal expansion and, possibly, reduction to $UO_{2.00}$. The lattice parameter should thus increase. The results obtained here surprisingly contradict this expectation, because a large lattice parameter decrease occurred between 350 K and 510 K. It remains quite small until 770 K. A comparison with reported thermal expansion data for $UO_{2+\delta}$ was made to clarify these results. By applying the thermal expansion coefficient (TEC) calculated by Yamashita et al. for $UO_{2.00}$[10] to the lattice parameters of $UO_{2+\delta}$ calculated as a function of δ from the Teske et al. relationship,[9] it is possible to give an approximation of $UO_{2+\delta}$ thermal expansion. This implies the hypothesis that the TEC remains constant, regardless of the O/M ratio, which was proposed by Martin[33] for O/M ratios up to 2.13, as well as between 2.23 and 2.25. As-calculated data and $U_4O_{9-\delta}$ (O/M ratios of 2.23−2.25) thermal expansion from Naito[34] are plotted in Figure 7, together with measured lattice parameters. Based on this plot, it seems that $UO_{2+\delta}$ is, in Domain I, oxidized to $U_4O_{9-\delta}$ (with an O/M ratio close to 2.23), which is unexpected considering the reducing atmosphere used. Because $U_4O_{9-\delta}$ has a structure very similar to that of $UO_{2+\delta}$, and is only a rearrangement of additional oxygen atoms, $UO_{2+\delta} \Leftrightarrow U_4O_{9-\delta}$ phase transformations are rendered possible even at such a relatively low temperature. It is highly likely that the oxygen excess associated with the reduction of $AmO_{2-\delta}$ to $Am_2O_{3+\delta}$ is seized by uranium cations to form the short-lived U_4O_9 phase within a limited temperature range.

IV.1.3. UO_2 and Am_2O_3 Behavior in Domains II and III (770 K < T < 1970 K). As observed in Figures 6 and 7, in Domains II and III, the uranium oxide lattice parameter returns to expected values and increases due to thermal expansion. $UO_{2+\delta}$ is almost stoichiometric between 770 K and 1870 K, because of the reducing atmosphere used. It even becomes hypostoichiometric above 1900 K, as previously reported.[35]

In the case of americium oxide, few but significant differences are observed in hexagonal A-type Am_2O_3 formation and thermal behavior. Its first peak emerges at 1320 K, with an intensity remaining relatively low, compared to that of the most intense UO_2 peak. Based on C-type Am_2O_3 peak shapes, even for such a low intensity (Figure 4), it can be considered that this phase was not formed at 1210 K, unlike in the single americium oxide sample. Even at a higher temperature, the intensities of the most intense hexagonal peaks remain less than 10% of those of UO_2 peaks, which is consistent with the low amount of americium oxide in the sample. Its maximum intensity is found at 1530 K and quickly decreases at higher temperature, which will be discussed in the next paragraph. Between 1840 and 1940 K, hexagonal A-type Am_2O_3 peaks completely vanish.

IV.2. $U_{1-x}Am_xO_{2\pm\delta}$ Solid-Solution Formation. *IV.2.1. Solid-Solution Emergence and Kinetic Aspects.* A second fluorite phase is only found above 1740 K with a lattice parameter (refined above 1840 K) slightly higher than that of UO_2 (5.593(1) Å vs 5.560(1) Å). The following observations allow identification of this phase as an emerging $U_{1-x}Am_xO_{2\pm\delta}$ solid solution:

- The lattice parameter difference is consistent with U(IV) substitution by Am(III), with the latter having a larger ionic radius than the former (1.09 Å vs 1.00 Å at VIII coordination[36]).
- The above-described behavior of americium oxide is also consistent with the formation of a solid solution: hexagonal Am_2O_3 peak intensities begin to decrease at 1620 K. In comparison, only a slight decrease was observed at 1740 K for a single americium oxide sample under the same conditions.[19] Thus, no significant sublimation is expected at such temperature, and the disappearance of the Am_2O_3 phase can be associated with americium insertion into a $U_{1-x}Am_xO_{2\pm\delta}$ solid solution.
- Furthermore, the decrease of A-type Am_2O_3 peak intensities coincides with the dropoff of UO_2 peaks,

dx.doi.org/10.1021/ic301124d | Inorg. Chem. 2012, 51, 9369−9375

which supports the assumption that they are caused by a common phenomenon, i.e., U/Am interdiffusion, leading to the emergence of a $U_{1-x}Am_xO_{2\pm\delta}$ phase. UO_2 logically vanishes at a slower rate than Am_2O_3, because of the greater amount of UO_2 in the starting powder mixture.

The solid solution is first observed at 1740 K. However, considering its similarity with the UO_2 phase and the slow kinetics at low temperature, it is possible that the formation of the solid solution may start at lower temperature. A similar sample underwent a thermal cycle with a plateau temperature of 1680 K for more than 6 h. The same behavior is observed for $UO_{2+\delta}$ (reduction to UO_2) and $AmO_{2-\delta}$ (reduction to hexagonal Am_2O_3), and an additional fluorite-type phase (i.e., $U_{1-x}Am_xO_{2\pm\delta}$) is observed at an early stage of the 1680-K plateau. The lower equivalent heating rate used in this experiment (~3.4 K min^{-1}, compared to 3.9 K min^{-1}) might have caused the earlier emergence of the solid solution, which confirms the influence of kinetic effects. Nevertheless, the main peaks of hexagonal A-type Am_2O_3 remains visible up to the end of the 1680 K plateau, though with very low intensity. At this temperature, the solid-solution formation cannot be complete, so two fluorite-type structures remain after the thermal treatment, one corresponding to UO_2, the other to a $U_{1-x}Am_xO_{2\pm\delta}$ with unknown δ and x values. Hence, the solid solution requires a temperature higher than 1700 K to properly form under these reducing sintering conditions, i.e., He/H_2 (5%).

Moreover, it is important to take into account that a powdered sample was used here. The direct comparison with phenomena occurring in a UO_2/AmO_2 pellet during reactive sintering is necessary. A pressed pellet offers more interaction surface between the two precursors. It also favors the occurrence, in the pellet porosities, of local atmospheres whose compositions are not controlled. Thus, it would not be surprising that, in a pellet sample, the full reduction of $AmO_{2-\delta}$ to C-type Am_2O_3 would be delayed due to the lower interaction with the reducing atmosphere. In contrast, the solid-solution formation might end faster, with U/Am interdiffusion being favored by the larger interaction surface.

IV.2.2. Discussion of Mechanisms Involved. Based on XAS measurements, Prieur et al. recently suggested two formation mechanisms to explain the complete reduction of Am(III) and the U(IV/V) mixed valence in a $U_{1-x}Am_xO_{2\pm\delta}$ solid solution.[6] In summary, the first one consists of the interdiffusion between $UO_{2+\delta}$ and $AmO_{2-\delta}$ followed by electron exchange between Am(IV) and U(IV), while the second implies the reduction of Am(IV) to Am(III) prior to the solid-solution formation. The present results clearly support the latter.

AmO_2 is first reduced to hexagonal A-type Am_2O_3 between 1000 K and 1500 K. Then, a reaction between Am_2O_3 and UO_2 occurs, leading to the formation of a fluorite-type phase exhibiting a lattice parameter higher than that of UO_2. Based on relative intensities of UO_2 and solid solution peaks, only a limited fraction of uranium may be integrated in the solid solution in the first step of the reaction. This indicates that the starting solid solution exhibits a relatively high proportion of americium. Furthermore, Am_2O_3 peak intensities decrease faster than those of UO_2. The former completely vanishes at 1940 K, whereas the latter only requires 4 h at 1970 K to disappear. This confirms that a $U_{1-x}Am_xO_{2\pm\delta}$ solid solution with an x-value higher than 0.15 is first formed and progressively diluted by UO_2.

Thus, the mechanism of the solid-solution formation is a reaction between two different structures, i.e., fluorite-type UO_2 and hexagonal A-type Am_2O_3. Uranium is expected to be nearly fully reduced to U(IV), according to the reducing atmosphere and the elevated temperature, while americium is present at the only valence state allowed by its A-type structure, i.e., Am(III).[12,18] The above-described reaction occurs not only between two different structures, but also through the interdiffusion of two cations exhibiting different, but stable, oxidation states. Uranium oxide is not known to exist at a lower valence than U(IV). Thus, the interdiffusion of Am(III) and U(IV) should lead to the emergence at a local range of a fluorite-type structure in order to accommodate both Am(III) and U(IV). Am_2O_3 and UO_2 are then progressively diluted in the solid solution. Considering the smaller ratio of americium in the sample, its full incorporation in the solid solution is faster.

IV.2.3. Final Solid Solution and O/M Ratio. At RT, the obtained solid solution can be considered as a $U_{1-x}Am_xO_{2\pm\delta}$ compound, with x close to 0.15. Its δ value remains unknown, since no convenient method to measure the O/M ratio of these materials was ever proposed. Its lattice parameter is equal to 5.480(1) Å, which is higher than those previously reported, all of which are smaller than that of $UO_{2.00}$ (5.4705 Å).[6,22,23,37] This large lattice parameter might be caused by the americium amount and the O/M (and at a lower level, the impurities from the $AmO_{2-\delta}$ powder), but decoupling these effects is not currently possible, because of the lack of data on this system. The only reported method to measure the O/M ratio is based on XAS measurements, through the determination of cationic charge distribution obtained from X-ray absorption near edge structure (XANES) spectra refinements.[23,37]

V. CONCLUSION

Recent XAS studies on $U_{1-x}Am_xO_{2\pm\delta}$ compounds presented an unexpected charge distribution: americium was found to be only trivalent, while a mixed valence (IV/V) was exhibited for uranium, regardless of Am content or sintering atmosphere. Based on these results, two formation mechanisms were proposed for this solid solution. On one hand, it could result from $UO_{2+\delta}/AmO_{2-\delta}$ interdiffusion, the charge distribution being achieved via an electron transfer once the solid solution is formed. On the other hand, Am(IV) reduction to Am(III) could occur before the reaction between uranium and americium oxides, the solid solution would thus be formed from $UO_{2+\delta}$ and Am_2O_3.

Solid-state formation of $U_{1-x}Am_xO_{2\pm\delta}$ solid solution under reducing atmosphere was studied in situ by high-temperature X-ray diffraction (HT-XRD) using a UO_2/AmO_2 (15%) powder mixture. Obtained results show that the reduction of fluorite-type $AmO_{2-\delta}$ to C-type cubic $Am_2O_{3+\delta}$, at relatively low temperatures (i.e., inferior to 700 K), leads to an oxidation of UO_2 to a short-lived $U_4O_{9-\delta}$. $UO_{2+\delta}$ is then reduced to an almost-stoichiometric compound, while the previously reported transformation of C-type $Am_2O_{3+\delta}$ to hexagonal A-type Am_2O_3 occurs and is complete at 1500 K. Starting at 1740 K, a new fluorite-type phase emerges, which corresponds to a $U_{1-x'}Am_{x'}O_{2\pm\delta}$ phase (with $x' > x$) coexisting with UO_2. The solid solution is thus formed through reaction between hexagonal $Am(III)_2O_3$ and fluorite-type $U(IV)O_2$ while, simultaneously, the Am_2O_3 phase is consumed by this reaction and quickly vanishes. This formation can be considered complete after 4 h at 1970 K, when the UO_2 phase is fully

dx.doi.org/10.1021/ic301124d | Inorg. Chem. 2012, 51, 9369−9375

incorporated in the solid solution. Thus, this work clearly evidence one of the two mechanisms previously suggested by Prieur et al.[6]

AUTHOR INFORMATION

Corresponding Author

*E-mail: thibaud.delahaye@cea.fr.

Notes

The authors declare no competing financial interest.

ACKNOWLEDGMENTS

The authors would like to thank M. Bataille and P. Coste for sample preparation, S. Caron for FEG-SEM observations, N. T. Reilly for her advice, and, more particularly, J. C. Richaud for HT-XRD sample handling and measurements. F. Lebreton and D. Prieur acknowledge the CEA program PACFA for financial support through Ph.D. funding.

REFERENCES

(1) Warin, D. *J. Nucl. Sci. Technol.* **2007**, *44*, 410−414.

(2) Lebreton, F.; Prieur, D.; Jankowiak, A.; Delahaye, T.; Tribet, M.; Donnet, L.; Dehaudt, P. *J. Nucl. Mater.* **2011**, *420*, 213−217.

(3) Prunier, C.; Broussard, F.; Koch, L.; Coquerelle, M. In *Proceedings of the Global '93 Conference*, Seattle, WA, 1993; pp 158−163.

(4) Prieur, D.; Jankowiak, A.; Delahaye, T.; Herlet, N.; Dehaudt, P.; Blanchart, P. *J. Nucl. Mater.* **2011**, *414*, 503−507.

(5) Carmarcat, N.; Garzenne, C.; Le Mer, J.; Leroyer, H.; Desroches, E.; Delbecq, J.-M. *C. R. Mec.* **2011**, *339*, 209−218.

(6) Prieur, D.; Martin, P. M.; Jankowiak, A.; Gavilan, E.; Scheinost, A. C.; Herlet, N.; Dehaudt, P.; Blanchart, P. *Inorg. Chem.* **2011**, *50*, 12437−12445.

(7) Prieur, D.; Lebreton, F.; Martin, P. M.; Jankowiak, A.; Delahaye, T.; Dehaudt, P.; Blanchart, P. *J. Eur. Ceram. Soc.* **2012**, *32*, 1585−1591.

(8) Delahaye, T.; Lebreton, F.; Horlait, D.; Herlet, N.; Dehaudt, P. Application of the UMACS process to highly dense $U_{1-x}Am_xO_{2\pm\delta}$ MABB Fuel Fabrication for the DIAMINO irradiation. *J. Nucl. Mater.* In press, **2012** (DOI: 10.1016/j.jnucmat.2012.07.018).

(9) Teske, K.; Ullmann, H.; Rettig, D. *J. Nucl. Mater.* **1983**, *116*, 260−266.

(10) Yamashita, T.; Nitani, N.; Tsuji, T.; Inagaki, H. *J. Nucl. Mater.* **1997**, *245*, 72−78.

(11) Hurtgen, C.; Fuger, J. *Inorg. Nucl. Chem. Lett.* **1977**, *13*, 179−188.

(12) Chikalla, T. D.; Eyring, L. J. *J. Inorg. Nucl. Chem.* **1968**, *30*, 133−145.

(13) Morss, L. R. *Handbook on the Physics and Chemistry of Rare Earths*, Vol. *18*; North−Holland Publishing: New York, 1994; pp 239−291.

(14) Willis, B. T. M. *Nature* **1963**, *197*, 755−756.

(15) Willis, B. T. M. *Acta Crystallogr., Sect. A: Cryst. Phys. Diffr., Theor. Gen. Crystallogr.* **1978**, *34*, 88−90.

(16) Yakub, E.; Ronchi, C.; Staicu, D. *J. Nucl. Mater.* **2009**, *389*, 119−126.

(17) Templeton, D. H.; Dauben, C. H. *J. Am. Ceram. Soc.* **1953**, *75*, 4560−4562.

(18) Sari, C.; Zamorani, E. *J. Nucl. Mater.* **1970**, *37*, 324−330.

(19) Lebreton, F.; Belin, R. C.; Delahaye, T.; Blanchart, P. In-situ XRD study of phase transformations in the Am−O system. *J. Solid State Chem.*, In Press (DOI: 10.1016/j.jssc.2012.06.027).

(20) Prieur, D.; Jankowiak, A.; Leorier, C.; Herlet, N.; Donnet, L.; Dehaudt, P.; Maillard, C.; Laval, J.-P.; Blanchart, P. *Powder Technol.* **2011**, *208*, 553−557.

(21) Prieur, D.; Jankowiak, A.; Lechelle, J.; Herlet, N.; Dehaudt, P.; Blanchart, P. *J. Nucl. Mater.* **2012**, *424*, 285−288.

(22) Nishi, T.; Nakada, M.; Suzuki, C.; Shibata, H.; Okamoto, Y.; Akabori, M.; Hirata, M. *J. Nucl. Mater.* **2011**, *418*, 311−312.

(23) Vespa, M.; Rini, M.; Spino, J.; Vitora, T.; Somers, J. *J. Nucl. Mater.* **2012**, *421*, 80−8.

(24) Fujino, T.; Yamashita, T.; Ohuchi, K.; Naito, K.; Tsuji, T. *J. Nucl. Mater.* **1993**, *202*, 154−162.

(25) Suzuki, C. Presented at *7th International Workshop on Materials Models and Simulations for Nuclear Fuels*, Karlsruhe, Germany, 2008.

(26) Kim, H. S.; Yoon, Y. K.; Lee, Y. W. *J. Nucl. Mater.* **1995**, *226*, 206−215.

(27) Fujino, T.; Sato, N.; Yamada, K. *J. Nucl. Mater.* **1995**, *223*, 6−19.

(28) Kim, J. G.; Ha, Y. K.; Park, S. D.; Jee, K. Y.; Kim, W.-H. *J. Nucl. Mater.* **2011**, *297*, 327−331.

(29) Ohmichi, T.; Fukushima, S.; Maeda, A.; Watanabe, H. *J. Nucl. Mater.* **1981**, *102*, 42−6.

(30) Hinatsu, Y.; Fujino, T. J. *Solid State Chem.* **1988**, *73*, 348−355.

(31) TOPAS V4: General profile and structure analysis software for powder diffraction data. User's manual; Bruker AXS: Karlsruhe, Germany, 2005.

(32) Wheeler, V. J.; Jones, I. G. *J. Nucl. Mater.* **1972**, *42*, 117−121.

(33) Martin, D. G. *J. Nucl. Mater.* **1988**, *152*, 94−101.

(34) Naito, K. *J. Nucl. Mater.* **1974**, *51*, 126−135.

(35) Guéneau, C.; Baichi, M.; Labroche, D.; Chatillon, C.; Sundman, B. *J. Nucl. Mater.* **2002**, *304*, 161−175.

(36) Shannon, R. D. *Acta Crystallogr., Sect. A: Cryst. Phys. Diffr., Theor. Gen. Crystallogr.* **1976**, *32*, 751−767.

(37) Prieur, D.; Martin, P.; Lebreton, F.; Delehaye, T.; Banerjee, D.; Scheinost, A. C.; Jankowiak, A. Accomodation of multivalent cations in fluorite-type solid solution: Case of Am-bearing UO_2. *Inorg. Chem.*, submitted for publication, **2012**.